http://www.scar.ac.cn
Sciences in Cold and Arid Regions
Volume 8, Issue 2, April, 2016

Citation: Li MS, Su ZB, Ma YM, *et al*., 2016. Characteristics of land-atmosphere energy and turbulent fluxes over the plateau steppe in central Tibetan Plateau. Sciences in Cold and Arid Regions, 8(2): 0103–0115. DOI: 10.3724/SP.J.1226.2016.00103.

Characteristics of land-atmosphere energy and turbulent fluxes over the plateau steppe in central Tibetan Plateau

MaoShan Li [1*], ZhongBo Su [2], YaoMing Ma [3], XueLong Chen [2], Lang Zhang [3], ZeYong Hu [1]

1. *Key Laboratory of Land Surface Process and Climate Change in Cold and Arid Regions, Cold and Arid Regions Environmental and Engineering Research Institute, Chinese Academy of Sciences, Lanzhou, Gansu 730000, China*
2. *Faculty of Geo-Information Science and Earth Observation of the University of Twente, Enschede, The Netherlands*
3. *Institute of Tibetan Plateau Research, Chinese Academy of Sciences, Beijing 100101, China*

*Correspondence to: MaoShan Li, Key Laboratory of Land Surface Process and Climate Change in Cold and Arid Regions, Cold and Arid Regions Environmental and Engineering Research Institute, Chinese Academy of Sciences. No. 320, West Donggang Road, Lanzhou, Gansu 730000, China. E-mail: mshli@lzb.ac.cn

Received: July 27, 2015 Accepted: November 23, 2015

ABSTRACT

The land-atmosphere energy and turbulence exchange is key to understanding land surface processes on the Tibetan Plateau (TP). Using observed data for Aug. 4 to Dec. 3, 2012 from the Bujiao observation point (BJ) of the Nagqu Plateau Climate and Environment Station (NPCE-BJ), different characteristics of the energy flux during the Asian summer monsoon (ASM) season and post-monsoon period were analyzed. This study outlines the impact of the ASM on energy fluxes in the central TP. It also demonstrates that the surface energy closure rate during the ASM season is higher than that of the post-monsoon period. Footprint modeling shows the distribution of data quality assessments (QA) and quality controls (QC) surrounding the observation point. The measured turbulent flux data at the NPCE-BJ site were highly representative of the target land-use type. The target surface contributed more to the fluxes under unstable conditions than under stable conditions. The main wind directions (180° and 210°) with the highest data density showed flux contributions reaching 100%, even under stable conditions. The lowest flux contributions were found in sectors with low data density, *e.g*., 90.4% in the 360° sector under stable conditions during the ASM season. Lastly, a surface energy water balance (SEWAB) model was used to gap-fill any absent or corrected turbulence data. The potential simulation error was also explored in this study. The Nash-Sutcliffe model efficiency coefficients (NSEs) of the observed fluxes with the SEWAB model runs were 0.78 for sensible heat flux and 0.63 for latent heat flux during the ASM season, but unrealistic values of −0.9 for latent heat flux during the post-monsoon period.

Keywords: turbulent energy flux; Asian summer monsoon; gap-filling; surface energy water balance model; central Tibetan Plateau

1 Introduction

The exchange of energy, momentum, and mass between land and atmosphere is key to understanding land surface processes, which in turn affect atmospheric circulation and climate. The Tibetan Plateau (TP) is the world's highest and largest alpine region, with altitudes of >4,000 m a.s.l. spanning 25° of longitude. Owing to its high altitude and its consequent enormous effect on the regional and global energy and water cycles, the TP has been the focus of climate study since the mid-1970s (Flohn, 1957; Yeh *et al*., 1957). A series of atmospheric science expeditions have been carried out on the TP, including the First

Tibetan Plateau Meteorological Science Experiment (1979), Tibetan Plateau Surface Heat Resource Observations (Ji *et al*., 1986), the Second Tibetan Plateau Meteorological Science Experiment (TIPEX) (Xu *et al*., 2002), and the Coordinated and Enhanced Observation Period (CEOP) of the Asian-Australian Monsoon Project in Tibet (CAMP-Tibet) (Koike *et al*., 1999; Wang *et al*., 1999; Ma *et al*., 2005; Ma *et al*., 2006). Recently, work by the Japan International Cooperation Agency (JICA) supported observations made on the TP and its surrounding areas. We have studied the effect of dynamic and heat transport from the TP on the climates of China, East Asia, and indeed the whole world using all these datasets. Our results indicated that sensible heat flux transfers prevail during the pre-monsoon periods, but during the ASM (Asian summer monsoon) seasons, latent heat flux predominates (excluding the western TP) (Chen *et al*., 1985). There were clear energy imbalances during the ASM seasons (Bian *et al*., 2002; Yang *et al*., 2004).

Previous studies have shown that, pre-ASM, the plateau surface is the major energy source providing sensible heat flux to the atmosphere (Li and Yanai, 1996). During the rainy season, the latent heat released to the atmosphere is the dominant heat source over the eastern TP, but sensible heat flux values are comparable to latent heat flux values over the western TP (Chen *et al*., 1985). Over the past 50 years, scientists have focused closely on research into energy and turbulent fluxes over the TP. The First Tibetan Plateau Meteorological Science Experiment (1979) obtained some important results: during dry periods, the sensible heat flux is the major energy source delivering heat to the atmosphere, whereas latent heat flux values are greater than sensible heat flux values in wet periods (Zhang *et al*., 1988).

Many observations of the TP ground surface (Ji *et al*., 1986) have improved our understanding of land-atmosphere interaction. In summer, the plateau surface is a heat source, and in dry periods the sensible heat flux is the major heat source; during the rainy season, the latent heat flux becomes as important as the sensible heat flux (Qian *et al*., 1997). Research shows that the ASM begins in June, is strongest in July, and retreats in October on the TP (Xu and Gao, 1962). The Bowen ratio (*Bo*) changes clearly with seasons on the TP; it is constant during the daytime before Sept. 27 (ASM season), then changes with time. We therefore studied the monsoonal effect on energy fluxes for the ASM season and post-monsoon period separately, following Wang *et al*. (2005). Although many energy unbalance studies have been performed, none of them definitively determined the reasons for energy unbalance. Li *et al*. (2015) produced a meta-analysis of flux measurements with a more climatological focus, which revealed a significant dependence of the energy balance components on the altitude and on the land-use types in the TP. Different stages of vegetation development and land cover density of grasslands can also lead to temporal variation of surface characteristics at a single site. The turbulent fluxes at an individual location are also influenced by these differences. Therefore, the first objective of this study was investigation of the flux and energy balance non-closure difference with changing time using observation data from the Nagqu Plateau Climate and Environment Station (NPCE-BJ) located in the center of the TP.

Footprint climatology analysis was applied to determine the contribution of target land use to total flux (Göckede *et al*., 2004, 2006; Rebmann *et al*., 2005). High mountains, lakes, ice, and grasslands are distributed over the whole TP. Accordingly, the second objective of the present study was to investigate the presentation of the data processing and quality control of the flux data.

During the long monitoring period, data gaps occurred due to various reasons. Therefore, this study needed a gap-filling method to address the missing data, so we used a 1-D soil-vegetation-atmosphere transfer scheme (surface energy water balance, or SEWAB) developed by Mengelkamp *et al*. (1999, 2001) to simulate the surface energy balance at the NPCE-BJ area, followed by statistical analysis to associate the biases and correlations between model outputs and observations.

2 Site description and experimental set-up

The Bujiao observation point (BJ) of the Nagqu Plateau Climate and Environment Station (NPCE-BJ) is located in the Nagqu area of the central TP. Its surface is essentially flat and open. Prior to the ASM period, the surface is very dry and covered by dry grass; with the onset of the ASM, the surface becomes wetter and the grass starts to grow rapidly. The NPCE-BJ station consists of an eddy covariance (EC) tower, an automatic weather station (AWS) for measuring radiation and wind speed, and a planet boundary layer (PBL) tower with a soil measurement system to enable the detection of all surface energy balance components. A land-use map of a 4km×4km area, with the location of the EC tower indicated as a black circle in the middle of the map, is given in Figure 1. The positions of the AWS and PBL tower near the EC tower are marked with a red cross.

A turbulent flux measurement sonic anemometer (CSAT3, Campbell Scientific, Inc.) was set up 3 m above the ground at the NPCE-BJ site (31.37°N, 91.9°E; 4,509 m a.s.1.). The precision of the measured horizontal wind speed was better than 0.04 m/s, while that of the vertical wind speed was better than 0.02

m/s. The density of water vapor (H_2O) and the concentration of carbon dioxide (CO_2) were obtained using an LI-7500 open-path gas analyzer (Li-COR Biosciences) for H_2O and CO_2 concentrations. This instrument responds quickly to the environment, and has been reliably used over long periods in the field. The data logging system used was the CR5000 control system (Campbell Scientific, Inc.). The measurement frequency of the EC system used was 10 Hz, and the flux data are output every 30 minutes. All EC data were processed and quality-controlled using the TK3.1 software package and produced turbulence datasets. Net radiation (R_{net}) short-wave components were measured with a CM21 device (Kipp & Zonen, B.V.), and long-wave components with an Eppley precision infrared radiometer (PIR) (Eppley Laboratory, Inc.) at a height of 1.40 m above the surface. Subsurface soil heat flux was recorded at 0.05 m and 0.10 m depths with an HFP01 heat flux plate (Hukseflux Thermal Sensors); the soil temperature at 0.05, 0.10, 0.20, 0.40, 0.80 and 1.60 m depths was measured with a TR219-L probe (Tri-Tronics), and the soil moisture at 0.05, 0.10, 0.20, 0.40, 0.80 and 1.60 m depths was measured using a CS616-L water content reflectometer (Campbell Scientific, Inc.). Precipitation was measured using a Geonor model T-200B precipitation weighing gauge (Geonor, Inc.), which allows the measurement of both liquid and solid precipitation.

Figure 1 Land-use map at the NPCE-BJ site

3 Turbulent data processing

3.1 TK3.1 processing

This research used observation data from Aug. 4 to Dec. 3, 2012 at the NPCE-BJ site. The EC flux values of the NPCE-BJ turbulence data were processed and quality-controlled using the TK3.1 software package, an update of TK3 (Mauder and Foken, 2011). The processing steps and flux corrections listed below were applied to the EC raw data following Mauder *et al*. (2006).

- Calculation of averages, variances, and covariances for using averaged 30-min intervals and taking into consideration the time delays between different sensors, and excluding physically invalid values and spikes (Vickers and Mahrt, 1997).
- Cross-wind correction of the sonic temperature.
- Planar fit coordinate rotation (Wilczak *et al*., 2001).
- Correction of spectral loss due to path-length averaging, spatial separation of the sensors, and the dynamic frequency effect of signals (Moore, 1986).
- Conversion of buoyancy into sensible heat flux (Schotanus *et al*., 1983; Liu *et al*., 2001).
- Correction of density fluctuations (WPL correction) to determine fluxes in the scalar quantities of H_2O and CO_2 (Webb *et al*., 1980; Fuehrer and Friehe, 2002; Liebethal and Foken, 2003, 2004).

The impact of these processing and flux-correction steps on flux estimates and C_{EB} (energy balance closure**)** has been discussed in Mauder *et al*. (2006). Previous quality tests implemented using TK3 consisted of a stationarity test and a test of the fulfilment of integral turbulence characteristics (ITC) for each turbulent flux (Foken and Wichura, 1996; Foken *et al*., 2004). According to Rebmann *et al*. (2005), the final quality flag (1–5) is assigned to a specific half-hourly turbulent flux value by combining the quality flags for stationarity and ITC. Classes 1–2 can be used for fundamental research and classes 3–4 for general use, such as continuously-running systems. Turbulent flux values marked with a class 5 quality flag should be rejected. This information is also provided in the NPCE-BJ turbulence database (Section 2) along with the footprint modeling results (Section 4.3 below).

3.2 Data selection

The following data selection criteria were applied to the results shown in Section 4 below. The data quality tests used is described in Section 3.1. Turbulent flux data within the following parameters were con-

sidered in this analysis:

- TK3.1 quality flags <3 (Section 3.1); and
- Flux contributions from the target land-use type >90% (Section 3.4 below).

3.3 Energy balance closure (C_{EB})

A possible residuum of the surface energy balance (Q_{res}) was evaluated at all the measuring sites in the turbulence network where additional radiation and soil measurements were carried out and turbulent fluxes of sensible heat (Q_H), and latent heat (Q_E) were measured. At the surface, the net radiation (Q_S), is transformed into Q_H and Q_E and into the ground heat flux (Q_G), thus:

$$-Q_S = Q_H + Q_E + Q_G + Q_{res} \quad (1)$$

The heat storage in the upper soil layer is included in the value of Q_G and was calculated according to the method of Yang and Wang (2008). Other storage terms (*e.g.*, plants, air) and photosynthesis can be neglected as they are usually very small for low-level vegetation (Foken, 2008).

Several studies have suggested a significant imbalance (10%–40%) in the TP's energy budget (Kim *et al.*, 2000; Bian *et al.*, 2002). Sensible and latent heat fluxes were therefore corrected following Twine *et al*. (2000) as suggested by Foken (2008): The energy balance residuum (Q_{res}) was distributed among the turbulent fluxes, while *Bo* was held steady; the energy balance correction method (EBC) was then employed to yield the corrected energy balance sensible ($Q_{H,EBC}$) and latent ($Q_{E,EBC}$) heat fluxes. In order to avoid unreasonably large corrections and artificial spikes, the correction was not applied when *Bo* was negative or if at least one of the turbulent fluxes failed to exceed the specified measurement of accuracy, which was assumed to be 10 W/m^2 in absolute terms. Instead, such values were excluded from further analysis. After filtering and energy balance correction were complete, missing values accounted for up to 42% of the $Q_{H,EBC}$ and $Q_{E,EBC}$ records. Most of these gaps, however, occurred during the night, when the fluxes were known to be low. Nonetheless, gap-filling was necessary to obtain unbiased mean diurnal or longer-period flux values. The influence of gap-filling on the overall results is discussed in Section 4.3 below.

3.4 Footprint modeling

In order to evaluate the spatial representation of the measured turbulent flux data in the context of underlying land-use distribution, a footprint model was applied to the NPCE-BJ EC flux site. Following the approach of Göckede *et al*. (2004, 2006), the flux data-quality flagging scheme of Rebmann *et al*. (2005) was combined with the Thomson (1987) 3-D Lagrangian stochastic trajectory Langevin-type model (Wilson and Sawford, 1996). The parameterization followed the flow statistics and the effect of stability on the profiles used in Rannik *et al*. (2003). The approach of Göckede *et al*. (2004, 2006) allows the determination of footprint climatology in relation to land use (spatial representation) and the spatial distribution of quality flags (spatial quality structure), as well as the percentage calculation of particular target land-use-type flux contributions to the total flux measured for each 30-min turbulent flux period. Recently, this flux data-quality evaluation approach was adapted for use in CarboEurope network sites by Rebmann *et al*. (2005) and Göckede *et al*. (2008).

Table 1 shows the flux contribution from the target land-use type at the NPCE-BJ station for different wind direction sectors and atmospheric conditions. Flux contributions from the target surface clearly increased as conditions moved from stable to unstable. The main wind directions (180° and 210°) with the highest data density (not shown) show flux contributions reaching 100%, even under stable conditions. The lowest flux contributions were found in sectors with low data density, *e.g.*, 90.4% in the 360° sector under stable conditions during the ASM season. Overall, the measured turbulent flux data at the NPCE-BJ site were highly representative of the target land-use type.

Table 1 Flux contributions from the "grass" target land-use type at the NPCE-BJ station from different wind direction sectors, and stability classes during monsoon season (upper) and post-monsoon (lower)

Season	Stability	Flux contribution from different wind direction sectors											
		30°	60°	90°	120°	150°	180°	210°	240°	270°	300°	330°	360°
Monsoon	Average flux contribution from target land-use type "grass" (%)												
	Stable	94.4	99.0	99.4	98.9	99.0	100	100	99.9	97.6	99.7	100	90.4
	Neutral	98.4	100	100	100	100	100	100	100	99.9	100	100	92.4
	Unstable	99.0	100	100	100	100	100	100	100	100	100	99.8	95.0
Post-monsoon	Average flux contribution from target land-use type "grass" (%)												
	Stable	93.3	98.7	98.7	98.4	98.7	100	100	99.9	98.6	99.8	100	90.8
	Neutral	96.4	99.9	99.9	100	100	100	100	100	100	100	99.9	93.2
	Unstable	98.7	100	100	100	100	100	100	100	100	100	99.8	96.3

3.5 SEWAB model set-up

Surface energy balance for the NPCE-BJ area was simulated using a 1-D soil-vegetation-atmosphere transfer scheme (surface energy water balance, or SEWAB) developed by Mengelkamp *et al*. (1999, 2001). This model was chosen due to its use of the C_{EB} technique, which was well-rated in a comparative study by Kracher *et al*. (2009). The model solves temperature and soil moisture distribution using a diffusion equation and the Richards equation, respectively. Soil moisture characteristics follow the relation given by Clapp and Hornberger (1978). Bulk approaches determine the turbulence exchange with the atmosphere, and account for atmospheric stability including aerodynamic and thermal roughness length as given by Louis (1979). The bulk latent heat flux (depending on the fraction of the surface covered by vegetation) is composed of evaporation from bare soil and wet foliage, and transpiration from dry leaves. The latter is governed by stomata resistance, parameterized in a Jarvis-type formulation according to Noilhan and Planton (1989). The energy balance equation is solved by iterating the surface temperature, and thus influencing individual balanced components, using Brent's method.

Land surface modeling on the TP faces specific problems caused by a marked variations in surface temperatures (Yang *et al*., 2009; Hong *et al*., 2010), likely triggering a diurnal cycle in the thermal roughness length (Ma *et al*., 2002; Yang *et al*., 2003), as well as large bare-soil evaporation typical of semi-arid areas (Agam *et al*., 2004; Balsamo *et al*., 2011). Adaptations include: (i) a variable thermal roughness length (Yang *et al*., 2008); (ii) calculation of soil thermal conductivity (Yang *et al*., 2005); and (iii) the parameterization of bare-soil evaporation (Mihailović *et al*., 1993). These changes have been incorporated into the model and tested at the alpine steppe site at Nam Co area in the central TP (Biermann *et al*., 2014).

Furthermore, all relevant model parameters have been inferred from field and laboratory measurements, an overview of which is given in Table 2. The optional hydrological modules of ponding, variable infiltration capacity (VIC), subsurface runoff, and base flow included in SEWAB were disabled. Half-hourly datasets from the NPCE-BJ site (Section 2), consisting of precipitation, air temperature, wind velocity, air pressure, relative humidity, and downwelling short-wave and long-wave radiation values, were applied to the model.

Table 2 Most important parameters for the model runs

Parameter	Value	Source
α	0.20	[a]
ε	0.97	Yang *et al*. (2009)
z_0 (m)	0.005	[a]
h_c (m)	0.05	[a]
f_{veg}	0.50	[a]
z_r (m)	0.10	[a]
LAI	1.0	Hu *et al*. (2009)
$R_{s,min}$ (s/m)	60	Alapaty *et al*. (1997)
R_{GL} (W/m^2)	100.0	Mengelkamp *et al*. (2001)
K_{sat} (m/s)	1.604×10^{-5}	[b]
Ψ_{sat} (m)	−0.30	[b]
η_{sat} (m^3/m^3)	0.372	[b]
η_{FC} (m^3/m^3)	0.18	[c], pF of 2.5 assumed
η_{WP} (m^3/m^3)	0.04	[c], pF of 4.5 assumed
b	3.25	[b]

Parameters for the BJ site are: albedo α, emissivity ε, roughness length z_0, canopy height h_c, fraction of vegetated area f_{veg}, rooting depth z_r, leaf area index *LAI*, minimum stomatal resistance $R_{s,min}$, radiation limit value for stomatal resistance R_{GL}, saturated hydraulic conductivity K_{sat}, matrix potential at saturation Ψ_{sat}, porosity η_{sat}, volumetric water content at field capacity η_{FC}, volumetric water content at wilting point η_{WP}, and exponent b for relationships (after Clapp and Hornberger, 1978). [a] measured/estimated in the field; [b] mean values from soil profile (laboratory) measurements (Chen *et al*., 2012); [c] inferred from Ψ_{sat}, porosity η_{sat}, and b according to Clapp and Hornberger (1978).

4 Results and discussion

4.1 Distribution of the surface energy fluxes and the energy balance closure in the central TP

Figure 2 shows the mean daily variations in surface energy fluxes during the ASM season (Figure 2a) and post-monsoon period (Figure 2b). When the ASM arrives, H_2O and evaporation values increase; Q_E is clearly dominant and exhibits values >200 W/m^2, higher than Q_H. Meanwhile, Q_G increases and reaches 200 W/m^2 at noon. A bell-shaped R_{net} curve is visible; R_{net} values at the NPCE-BJ site decrease within 12:00–14:00 as a result of the presence of convective

clouds. Conversely, Q_H is higher than Q_E during the post-monsoon period (Figure 2b). The residuum (Equation *(1)*) is smaller during the ASM season than during the post-monsoon period. It seems to depend on the ground heat flux, which is higher in the wet season, and is related both to a greater radiation input and to a thermal decoupling of dry soils during the post-monsoon period.

Several studies of turbulence structure have been conducted on the TP (Qi *et al*., 1996; Ma *et al*., 2002). Yeh and Gao (1979) obtained a vertically-integrated mean heat source of 138 W/m^2 over the western TP in June, but this was estimated to be 37 W/m^2 by Chen *et al.* in 1985. This large discrepancy was caused by the different drag coefficients used in the bulk method, resulting in sensible heat flux values differing by a factor of 3 to 4. Li *et al.* (2001) reported a wide range of drag coefficients (2.5×10^{-3} to 12×10^{-3}) over the TP despite the use of the same data.

Surface energy latent heat flux can be estimated as a budget residue. However, this approach is prone to error because a significant imbalance in the TP's energy budget (10%–40%) has been reported (Kim *et al.*, 2000; Bian *et al.*, 2002). Figure 3 shows that over the TP, C_{EB} is 88% during the ASM season (Figure 3a) and 72% during the post-monsoon period (Figure 3b). This is higher than the values reported by Kim *et al.* (2000) and Bian *et al.* (2002) (residuum: 10%–40%). However, there was a residuum of 10%–30% at the NPCE-BJ station.

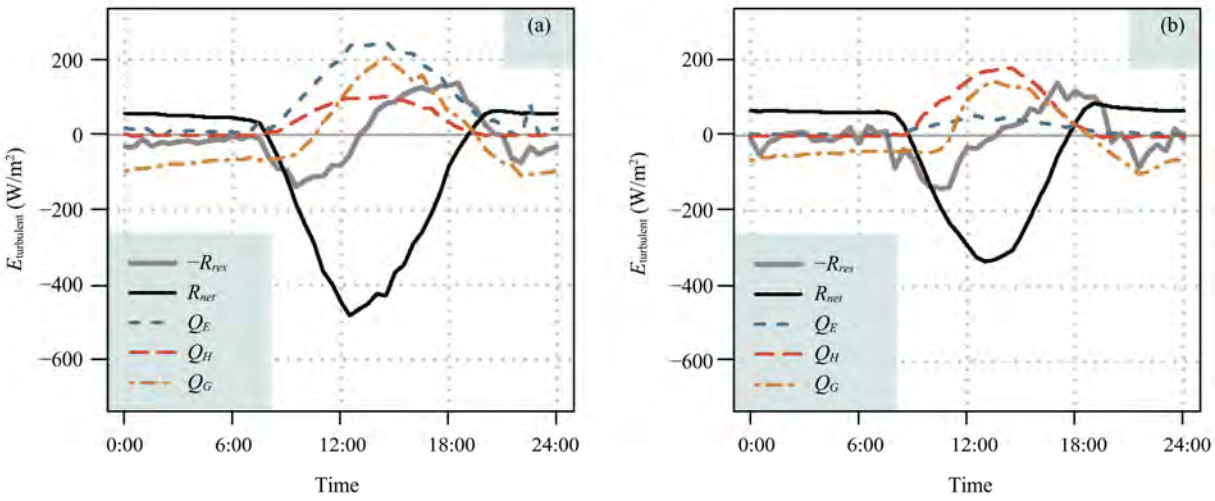

Figure 2 Surface averaged net radiation R_{net} and turbulent heat fluxes: averaged sensible heat flux (Q_H) , averaged latent heat flux (Q_E), and averaged ground heat flux (Q_G) during monsoon season (a) and post-monsoon period (b) at the NPCE-BJ site. $-R_{res}$ is the residuum of the energy flux

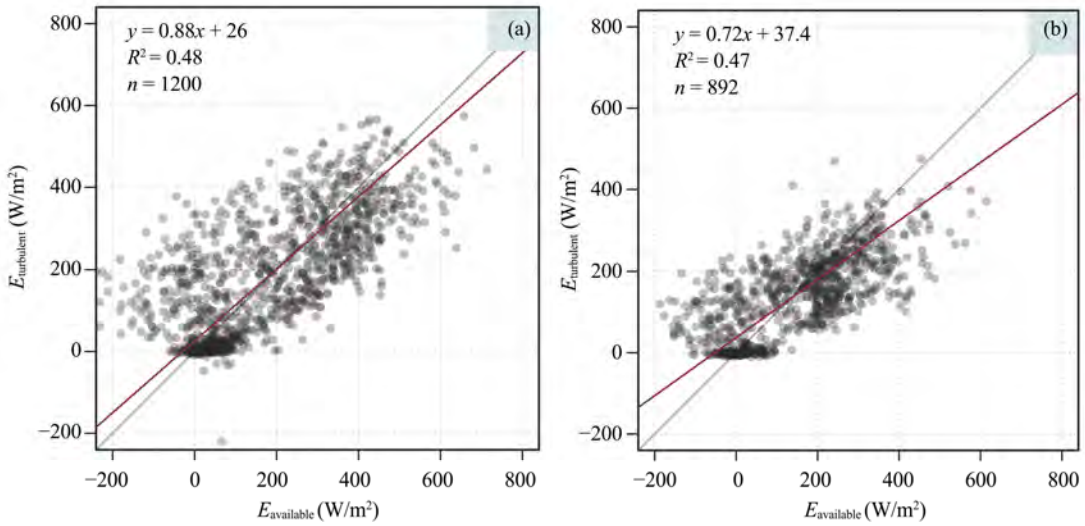

Figure 3 The energy balance closure during monsoon season (a) and post-monsoon season (b) at the NPCE-BJ station. The fitted equation is for the red line

4.2 Footprint modeling and quality checks

First, roughness lengths and land use were determined for a 10-m grid size for an area of approximately 4km×4km. Land-use classification was derived from visual inspection and Landsat TM imagery. The observation tower was located at the center of the investigation area.

To produce a cumulative flux data quality category for the NPCE-BJ site, the results of footprint calculations were combined with the quality-assessed turbulent flux data to give 2-D matrices. These matrices showed the dominant data quality class for each of the grid cells of the matrix surrounding the tower, and could be combined to give their contribution to the total flux.

Figure 4 shows that the cumulative flux contribution (isolines) over the observation period for the NPCE-BJ site consisted of 2,687 (ASM season) and 4,559 (post-monsoon) half-hourly datasets alongside the different land-use classes. Stable, neutral, and unstable atmospheric conditions were taken into account, but only 27% (ASM season) and 33% (post-monsoon period) of the cases were stable (when ζ >0.0625, ζ is obtained from

$$\zeta = (z_m - d)/L \qquad (2)$$

where z_m is observation height, d is zero plane displacement, and L is the Monin-Obukhov length). The features investigated within the source area *vis-à-vis* data quality were momentum flux, sensible heat flux, latent heat flux, CO_2 flux, and the contribution of land-use type to the total flux measured.

In Figure 4, the accumulation of the source weight functions for individual measurements taken over an ASM season and post-monsoon period at the NPCE-BJ site is illustrated for mixed, unstable, neutral, and stable atmospheric conditions, respectively. The background shows the land-use distribution that was applied to determine the contributions of different land-use classes to the total measured flux. The black lines on both figures are isolines, which reproduce the 3-D structure of the accumulated source weight function. The figures reveal that the small region close to the mast was of principal importance for the measurement site, while the furthest-removed region exerted only a minor influence during the ASM season or the post-monsoon period. The land-use classes were low-grass, wetland, riverbed, water, building, and hill (Figure 4).

In Figure 5, the colored flags show the dominant data quality flag for momentum flux during the ASM season (left) and the post-monsoon period (right), while the black isolines specify the relative flux contributions for the NPCE-BJ site. Blue flags indicate the highest flux data quality, while red flags indicate poor data quality. Sixty-two percent of the data are of high quality *vis-à-vis* momentum flux during the ASM season; this figure is 59% for the post-monsoon period (see Table 3). The overall data quality for momentum flux was highest under unstable atmospheric conditions during both periods. Under stable conditions, the overall quality of momentum flux was intermediate in the regions northwest of the tower. The worst-quality data in windy sectors and under stable conditions was found in hill and wetland areas.

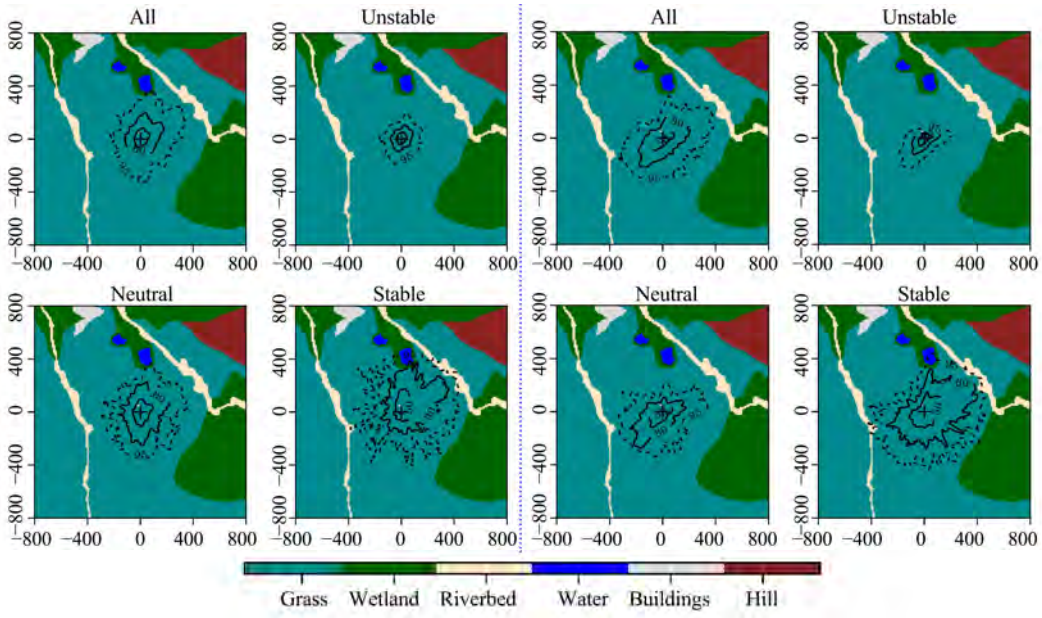

Figure 4 Spatial distribution of the land-use classifications combined with their relative flux contribution in the Nagqu area under all stratification conditions, unstable stratification, neutral stratification, and stable stratification during the monsoon season (left) and post-monsoon (right). Black isolines indicate the rate of the flux contribution, with 50%, 80%, and 95% from inside to outside, respectively. '+' is the location of the BJ station

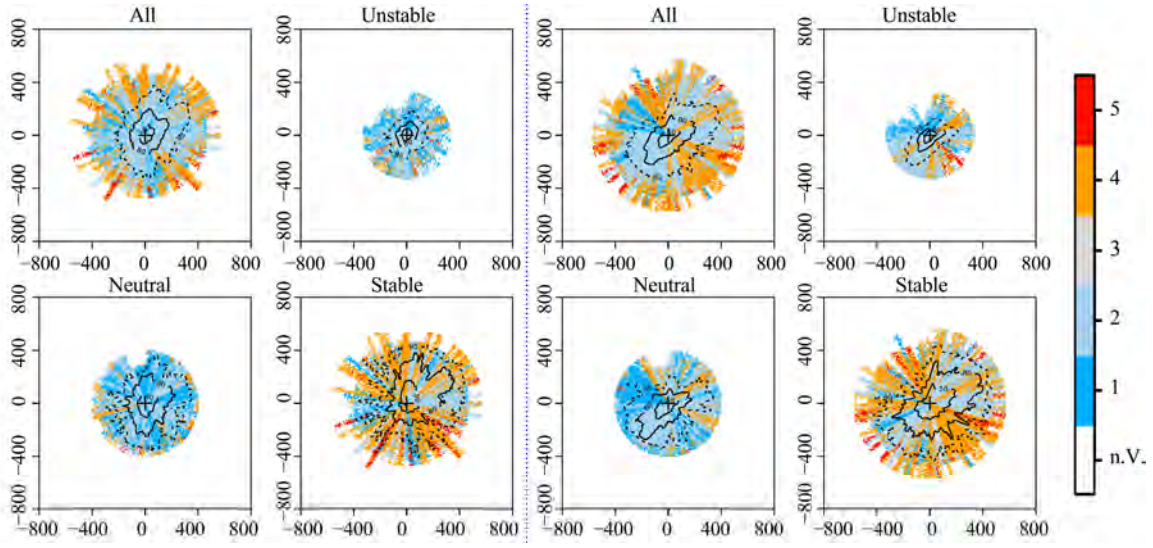

Figure 5 Spatial distribution of the data quality for the momentum at the NPCE-BJ site under different atmospheric stratifications during the monsoon season (left) and post-monsoon (right). Black isolines indicate the flux contribution for the sink area, with 50%, 80%, and 95% from inside to outside, respectively. '+' is the location of the BJ station

Table 3 Quality test for the fluxes of momentum τ (including integral turbulence characteristics), sensible heat Q_H, latent heat Q_E, and carbon dioxide flux F_{CO_2} (only for stationarity and the ITC test for σw) during monsoon (upper) and post-monsoon (lower). Numbers are relative to the total number of investigated cases for the NPCE-BJ site, in %

Monsoon season				
	τ flag 1-2	Q_H flag 1-2	Q_E flag 1-2	F_{CO_2} flag 1-2
Unstable	27	30	35	32
Neutral	23	9	20	14
Stable	12	3	13	9
All	62	42	68	55
Post-monsoon				
	τ flag 1-2	Q_H flag 1-2	Q_E flag 1-2	F_{CO_2} flag 1-2
Unstable	23	21	22	26
Neutral	22	15	13	17
Stable	14	2	9	9
All	59	38	44	52

The quality flags for sensible heat flux were derived from a combination of stationarity of the covariance and the integral turbulence characteristics of the vertical wind w and temperature T. As mentioned above, the integral turbulence characteristics of T do not yet have a valid parameterization for neutral and stable atmospheric conditions (Figure 6). The measured values agreed with the parameterization only under unstable conditions. Moreover, grids west and south of the tower had class 1 to 2 quality flags, whereas other areas had class 3 to 5 flags. The stationarity of the covariance often showed high data quality, but non-stationarity usually applied to the sensible heat flux of heterogeneous surfaces. The area east of the tower was influenced by a non-stationarity of sensible heat flux, and was also probably influenced by a distant wetland area (Figure 4). The roughness lengths of these latter areas were very different from the low grassland areas, and therefore had different heat exchange properties, explaining the non-stationarities of the covariance. Conversely, under neutral or stable atmospheric conditions, parameterization of the integral turbulence characteristics of T was probably not comparable to the literature (Li *et al.*, 2006).

The quality flags for latent flux were derived from a combination of the stationarity of the covariance and the integral turbulence characteristics of the vertical wind component w. The focus here is only on stationarity, as the integral turbulence characteristics of w are seldom negatively influenced and have already been investigated with momentum flux. Most cases were in the highest quality (blue-flag) class and occurred under unstable atmospheric conditions. As with sensible

heat flux, the latent heat flux in the area east of the tower was influenced by non-stationarity. The non-stationarities of the covariance in this area were probably influenced by a distant wetland area (Figure 7), which had a different roughness length and heat exchange properties.

Concerning the carbon dioxide (CO_2) flux, we focused only on stationarity. Fifty-five percent of the data during the ASM season were of high quality, falling to 52% during the post-monsoon period. These data mostly referred to stable atmospheric conditions during the post-monsoon period. Overall, most high-quality data were obtained under unstable atmospheric conditions. During the ASM season, some lower-quality data were collected far from the tower, which had originated east of the tower during the post-monsoon period. Under stable atmospheric conditions, only 9% of all the data were high quality during both periods. Under neutral atmospheric conditions, the data quality was higher during the post-monsoon period than in the ASM season. Lower-quality measurements came from east of the tower, as was the case with unstable atmospheric conditions. These results can be explained by the influence of a complicated topography on the area east of the flux tower (Figure 8).

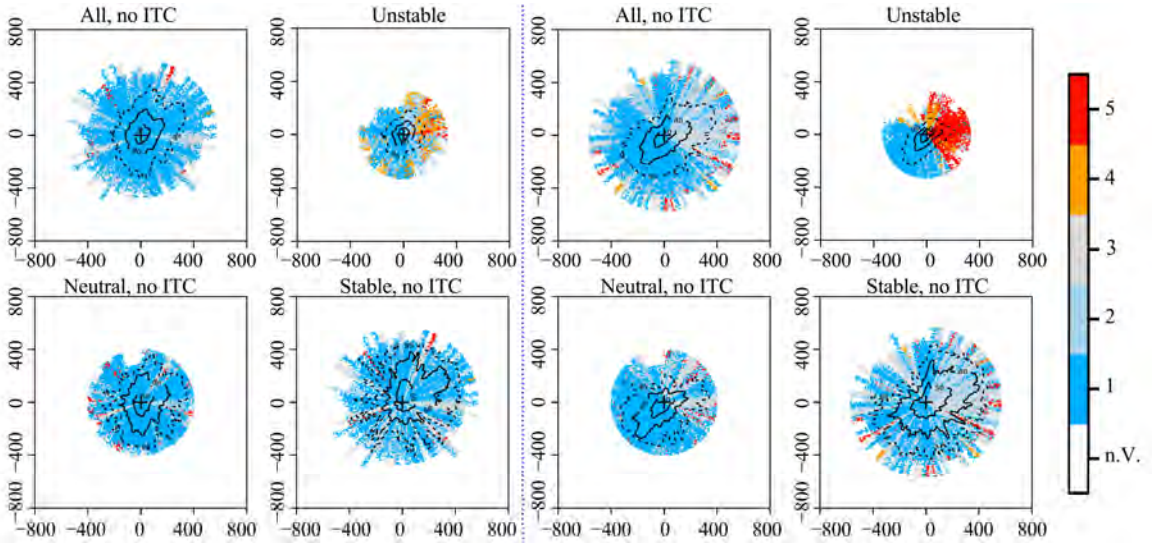

Figure 6 Spatial distribution of the data quality for the sensible heat flux at the NPCE-BJ site under different atmospheric stratifications during the monsoon season (left) and post-monsoon (right). Black isolines indicate the flux contribution for the sink area with 50%, 80%, and 95% from inside to outside, respectively. '+' is the location of the BJ station

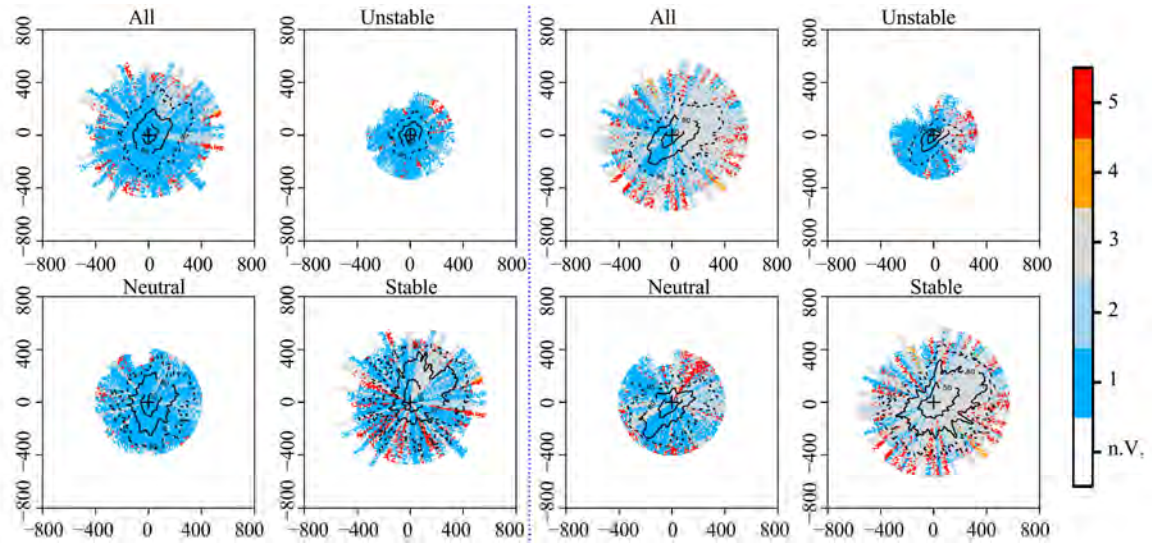

Figure 7 Spatial distribution of the data quality for the latent heat flux at the NPCE-BJ site under different atmospheric stratifications during the monsoon season (left) and post-monsoon (right). Black isolines indicate the flux contribution for the sink area, with 50%, 80%, and 95% from inside to outside, respectively. '+' is the location of the BJ station

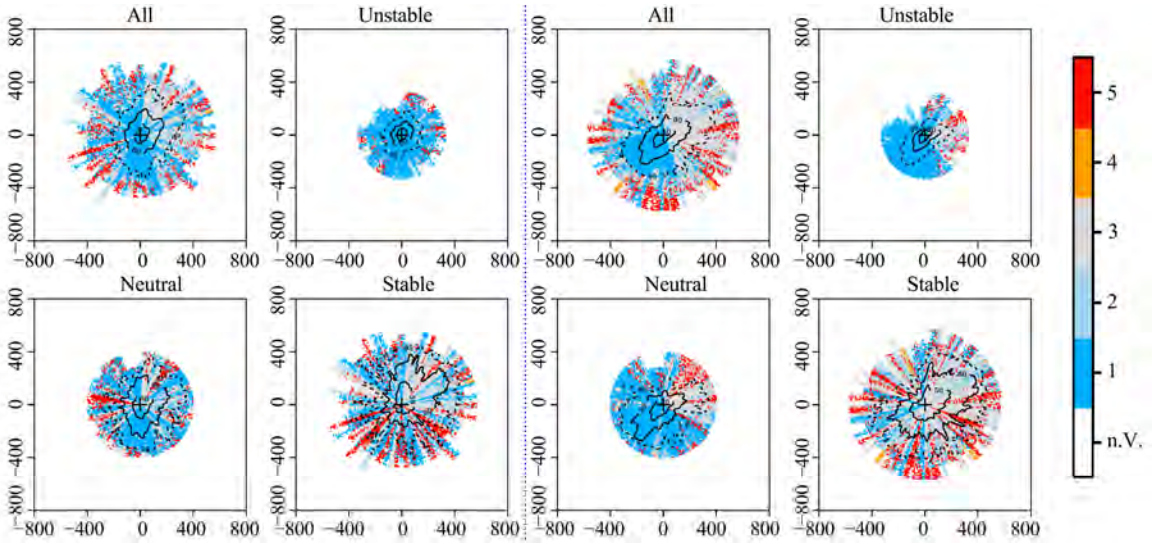

Figure 8 Spatial distribution of the data quality for the carbon dioxide (CO_2) flux at the NPCE-BJ site under different atmospheric stratifications during monsoon season (left) and post-monsoon (right). Black isolines indicate the flux contribution for the sink, with 50%, 80%, and 95% from inside to outside, respectively. '+' is the location of BJ station

4.3 Simulation results

We evaluated model performance using the Nash-Sutcliffe coefficient (NS; Nash and Sutcliffe, 1970), as follows:

$$NS = 1 - \frac{\sum_{i=1}^{N}(P_i - O_i)^2}{\sum_{i=1}^{N}(O_i - \overline{O})^2} \quad (3)$$

where O is the observation, P the model prediction, and $\overline{O}$ the observational mean.

Figure 9 shows the observed fluxes versus the SEWAB model runs. The NS coefficient (Equation *(3)*), shows reasonable fits for the NPCE-BJ site, with values of 0.78 for sensible heat flux and 0.63 for latent heat flux during the ASM season, but unrealistic values of −0.9 for latent heat flux during the post-monsoon period. To ensure a consistent averaging for long-term fluxes, all observed fluxes were gap-filled with the running model results. While this practice is necessary for providing average values, some bias is likely to be introduced during the evaluation and will become evident when comparing model runs with observed data, including the gap-filled values derived from the SEWAB model runs. The challenge remains to gap-fill the post-monsoon period's latent heat flux.

5 Summary and conclusions

In this study, the impact of the ASM on turbulence, footprint climatology, and simulation models at the NPCE-BJ site was analyzed. The results were as follows:

1) During the ASM season, latent heat flux was higher than sensible heat flux, and the energy closure rate was higher than that during the post-monsoon period. The lower C_{EB} values resulted from a low exchange of H_2O caused by negative air temperatures and low ground heat flux values due to frozen soil during the post-monsoon period.

2) Footprint models helped to identify the flux tower's footprint sectors. These models may have lower measuring certainties under certain atmospheric conditions. The measured turbulent flux data at the NPCE-BJ site were highly representative of the target land-use type. The target surface contributed more to the fluxes under unstable conditions than under stable conditions. The main wind directions (180° and 210°) with the highest data density showed flux contributions reaching 100%, even under stable conditions. The lowest flux contributions were found in sectors with low data density, *e.g.*, 90.4% in the 360° sector under stable conditions during the ASM season. Flux sites were often established in non-ideal terrain because of the limitations of nonhomogeneous underlying surfaces. Minor low-quality flux data were rejected and replaced by gap-filling procedures, as is usually done for fluxes under low-turbulence conditions. In the distribution patterns of all the fluxes, most high-quality data were attained under unstable conditions. During the ASM season, some lower-quality data were observed at a considerable distance from the tower, but just east of the tower during the post-monsoon period. Under stable conditions, both periods produced high-quality datasets for about 9% of all of the data. Under neutral conditions, the data quality during the post-monsoon period was higher than during the ASM season. Lower-quality measurements were found east of the tower,

as under unstable conditions. These resulted from the complex topography east of the flux tower.

3) Using the modeled results to gap-fill missing data, more realistic values were obtained for sensible heat flux than for latent heat flux. This method is feasible for the ASM season, but needs to be used with caution when gap-filling the latent heat flux data for the post-monsoon period. Modeling uncertainty results from the thermal and hydrological exchange parameterization included in SEWAB. This study provides a method for reducing such uncertainty.

There are many reasons for an imbalance in energy flux in heterogeneous underlying surfaces. For example, frozen soil processes were not considered in the SEWAB model for the post-monsoon period, a fact which would certainly influence final soil heat flux and energy imbalance. The calculation of soil heat flux now needs to be improved.

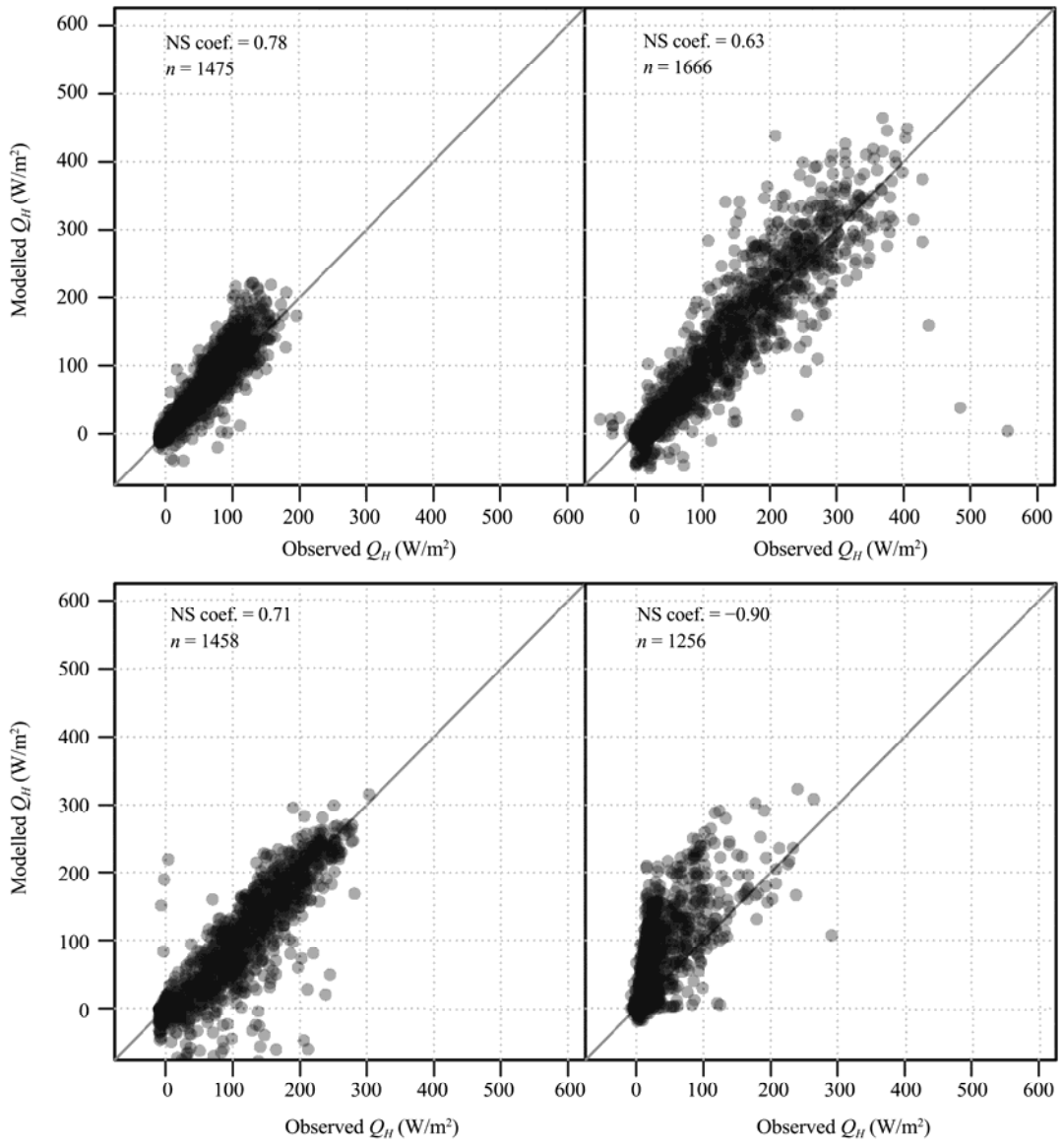

Figure 9 Energy balance corrected fluxes vs. optimized model runs, subjected to gap-filling for the NPCE-BJ station; the sensible heat flux and the latent heat flux from left to right during the monsoon season (upper) and post-monsoon (lower); *n* is the number of available observations and *NS* is the Nash-Sutcliffe coefficient

Acknowledgments:
This work was supported by the National Natural Science Foundation of China (Grant Nos. 91337212, 41175008), Cold and Arid Regions Environmental and Engineering Research Institute Youth Science Technology Service Network initiative (STS), the China Exchange Project (Grant No. 13CDP007), and the National Natural Science Foundation of China (Grant Nos. 40825015 and 40675012). The authors thank all colleagues and engineers who contributed to

the field observations at the NPCE-BJ station.

References:

Agam N, Berliner PR, Zangvil A, *et al.*, 2004. Soil water evaporation during the dry season in an arid zone. Journal of Geophysical Research, 109(D16): D16103. DOI: 10.1029/2004JD004802.

Alapaty K, Pleim JE, Raman S, *et al.*, 1997. Simulation of atmospheric boundary layer processes using local- and nonlocal-closure schemes. Journal of Applied Meteorology, 36(3): 214–233. DOI: 10.1175/1520-0450(1997)036<0214:SOABLP>2.0.CO;2.

Balsamo G, Boussetta S, Dutra E, *et al.*, 2011. Evolution of land surface processes in the IFS. ECMWF Newsletter, 127: 17–22.

Bian LG, Gao ZQ, Xu QD, *et al.*, 2002. Measurements of turbulence transfer in the near-surface layer over the southeastern Tibetan Plateau. Boundary-Layer Meteorology, 102: 281–300. DOI: 10.1023/A:1013177629245.

Biermann T, Babel W, Ma W, *et al.*, 2014. Turbulent flux observations and modelling over a shallow lake and a wet grassland in the Nam Co basin, Tibetan Plateau. Theoretical and Applied Climatology, 116: 301–316. DOI: 10.1007/s00704-013-0953-6.

Chen LX, Reiter ER, Feng ZQ, 1985. The atmosphere heat source over the Tibetan Plateau: May August 1979. Monthly Weather Review, 113: 1771–1790.

Chen YY, Yang K, Tang WJ, *et al.*, 2012. Parameterizing soil organic carbon's impacts on soil porosity and thermal parameters for Eastern Tibet grasslands. Science China (Earth Sciences), 55: 1001–1011. DOI: 10.1007/s11430-012-4433-0.

Clapp RB, Hornberger GM, 1978. Empirical equations for some soil hydraulic properties. Water Resources Research, 14(4): 601–604.

Flohn H, 1957. Large-scale aspects of the "summer monsoon" in South and East Asia. Journal of the Meteorological Society of Japan, 75: 180–186.

Foken T, 2008. The energy balance closure problem: An overview. Ecological Applications, 18: 1351–1367. DOI: 10.1890/06-0922.1.

Foken T, Göckede M, Mauder M, *et al.*, 2004. Post-field data quality control. In: Lee X, Massman W, Law B (eds.). Handbook of Micrometeorology: A Guide for Surface Flux Measurement and Analysis. Kluwer: Dordrecht, pp. 181–208.

Foken T, Wichura B, 1996. Tools for quality assessment of surface-based flux measurements. Agricultural and Forest Meteorology, 78: 83–105.

Fuehrer PL, Friehe CA, 2002. Flux corrections revisited. Boundary-Layer Meteorology, 102: 415–457.

Göckede M, Foken T, Aubinet M, *et al.*, 2008. Quality control of CarboEurope flux data, Part 1: Coupling footprint analyses with flux data quality assessment to evaluate sites in forest ecosystems. Biogeosciences, 5: 433–450.

Göckede M, Markkanen T, Hasager CB, *et al.*, 2006. Update of a footprint-based approach for the characterization of complex measurement sites. Boundary-Layer Meteorology, 118: 635–655. DOI: 10.1007/s10546-005-6435-3.

Göckede M, Rebmann C, Foken T, 2004. A combination of quality assessment tools for eddy covariance measurements with footprint modelling for the characterization of complex sites. Agricultural and Forest Meteorology, 127(3): 175–188. DOI: 10.1016/j.agrformet.2004.07.012.

Hong J, Kim J, Ishikawa H, *et al.*, 2010. Surface layer similarity in the nocturnal boundary layer: the application of Hilbert-Huang transform. Biogeosciences, 7: 1271–1278.

Hu ZM, Yu GT, Zhou YL, *et al.*, 2009. Partitioning of evapotranspiration and its controls in four grassland ecosystems: Application of a two-source model. Agricultural and Forest Meteorology, 149(9): 1410–1420. DOI: 10.1016/j.agrformet.2009.03.014.

Ji GL, Yao LC, Yuan FM, *et al.*, 1986. Characteristics of surface and atmosphere heating field over the Tibetan Plateau in winter in 1982. Science in China (B), 31(8): 876–888.

Kim J, Choi T, Lee H, *et al.*, 2000. Energy partitioning and its imbalance over a prairie site in central Tibetan Plateau during GAPE-IOP 1998. Supplement Eos, Transactions, American Geophyical Union, 81(22): 5.

Koike T, Yasunari T, Wang J, *et al.*, 1999. GAME-Tibet IOP Summary Report. Paper presented at the 1st International Workshop on GAME-Tibet, Xi'an, China.

Kracher D, Mengelkamp HT, Foken T, 2009. The residual of the energy balance closure and its influence on the results of three SVAT models. Meteorologische Zeitschrift, 18: 1–15. DOI: 10.1127/0941-2948/2009/0412.

Li CF, Yanai M, 1996. The onset and interannual variability of the Asian Summer Monsoon in relation to land–sea thermal contrast. Journal of Climate, 9: 358–375. DOI: http://dx.doi.org/10.1175/1520-0442(1996)009<0358:TOAIVO>2.0.CO;2.

Li GP, Duan TY, Haginoya S, *et al.*, 2001. Estimates of the bulk transfer coefficients and surface fluxes over the Tibetan Plateau using AWS data. Journal of the Meteorological Society of Japan, 79(2): 625–635. DOI: 10.2151/jmsj.79.625.

Li MS, Babel W, Chen XL, *et al.*, 2015. A 3-year data set of sensible and latent heat fluxes derived using eddy-covariance measurements on the Tibetan Plateau. Theoretical and Applied Climatology, 122: 457–469. DOI: 10.1007/s00704-014-1302-0.

Li MS, Ma YM, Ma WQ, *et al.*, 2006, Analysis of turbulent characteristics over the northern Tibetan Plateau area. Advances in Atmospheric Sciences, 23(4): 579–585.

Liebethal C, Foken T, 2003. On the significance of the Webb correction to fluxes. Boundary-Layer Meteorology, 109: 99–106.

Liebethal C, Foken T, 2004. On the significance of the Webb correction to fluxes. Corrigendum. Boundary-Layer Meteorology, 113: Heft 2.–S. 301.

Liu HP, Peters G, Foken T, 2001. New equations for sonic temperature variance and buoyancy heat flux with an omnidirectional sonic anemometer. Boundary-Layer Meteorology, 100: 459–468.

Louis JF, 1979. A parametric model of vertical fluxes in the atmosphere. Boundary-Layer Meteorology, 17: 187–202.

Ma YM, Fan SH, Ishikawa H, *et al.*, 2005. Diurnal and inter-monthly variation of land surface heat fluxes over the central Tibetan Plateau area. Theoretical and Applied Climatology, 80(2–4): 259–273. DOI: 10.1007/s00704-004-0104-1.

Ma YM, Tsukamoto O, Wang J, *et al.*, 2002. Analysis of aerodynamic and thermodynamic parameters on the grassy marshland surface of Tibetan Plateau. Progress in Natural Science, 12: 36–40.

Ma YM, Zhong L, Su Z, 2006. Determination of regional distributions and seasonal variations of land surface heat fluxes from Landsat-7 ETM data over the central Tibetan Plateau area. Journal of Geophysical Research, 111: D10305. DOI: 10.1029/2005JD006742.

Mauder M, Foken T, 2011. Documentation and instruction manual of the eddy covariance software package TK3. Work Report.

University of Bayreuth, Dept. of Micrometeorology, ISSN: 1614–8916, pp. 46–58.

Mauder M, Liebethal C, Göckede M, *et al.*, 2006. Processing and quality control of flux data during LITFASS-2003. Boundary-Layer Meteorology, 121: 67–88.

Mengelkamp H, Warrach K, Raschke E, 1999. SEWAB— a parameterization of the Surface Energy and Water Balance for atmospheric and hydrologic models. Advances in Water Resources, 23: 165–175. DOI: 10.1016/S0309-1708(99)00020-2.

Mengelkamp HT, Kiely G, Warrach K, 2001. Evaluation of the hydrological components added to an atmospheric land-surface scheme. Theoretical and Applied Climatology, 69(3–4): 199–212. DOI: 10.1007/s007040170025.

Mihailović DT, Pielke RA, Rajković B, *et al.*, 1993. A resistance representation of schemes for evaporation from bare and partly plant-covered surfaces for use in atmospheric model. Journal of Applied Meteorology, 32: 1038–1054.

Moore CJ, 1986. Frequency response corrections for eddy correlation systems. Boundary-Layer Meteorology, 37: 17–35.

Nash JE, Sutcliffe JV, 1970. River flow forecasting through conceptual models part I— A discussion of principles. Journal of Hydrology, 10: 282–290.

Noilhan J, Planton S, 1989. A simple parameterization of land surface processes for meteorological models. Monthly Weather Review, 117: 536–549. DOI: 10.1175/1520-0493(1989)117 <0536:ASPOLS>2.0.CO;2.

Qi YQ, Wang JM, Jia L, *et al.*, 1996. A study of turbulent transform characteristics in Wu daoliang area of Qinghai–Xizang Plateau. Plateau Meteorology, 15(2): 172–174.

Qian ZA, Jiao YJ, 1997. Advances and problems on Qinghai-Xizang Plateau meteorology research. Advances in Earth Sciences, 12(31): 207–216.

Rannik Ü, Markkanen T, Raittila J, *et al.*, 2003. Turbulence statistics inside and over forest: Influence on footprint prediction. Boundary-Layer Meteorology, 109: 163–189.

Rebmann C, Göckede M, Foken T, *et al.*, 2005. Quality analysis applied on eddy covariance measurements at complex forest sites using footprint modelling. Theoretical and Applied Climatology, 80: 121–141. DOI: 10.1007/s00704-004-0095-y.

Schotanus P, Nieuwstadt FTM, DeBruin H, 1983. Temperature measurement with a sonic anemometer and its application to heat and moisture fluxes. Boundary-Layer Meteorology, 26: 81–93.

Thomson DJ, 1987. Criteria for the selection of stochastic models of particle trajectories in turbulent flows. Journal of Fluid Mechanics, 180: 529–556.

Twine TE, Kustas WP, Norman JM, *et al.*, 2000. Correcting eddy-covariance flux underestimates over a grassland. Agricultural and Forest Meteorology, 103: 279–300. DOI: 10.1016/S0168-1923(00)00123-4.

Vickers D, Mahrt L, 1997. Quality control and flux sampling problems for tower and aircraft data. Journal of Atmospheric and Oceanic Technology, 14: 512–526.

Wang JM, Kim J, Liou YA, *et al.*, 1999. Energy balance analysis and one-dimensional simulation of land surface process in a short-grass site of Central Tibetan Plateau. Proceedings of the 1st International Workshop on GAME-Tibet, pp. 73–76.

Wang SW, Zhao ZC, Gong DY, *et al.*, 2005. Introduction to Modern Climate. Beijing: Meteorological Press, pp. 241.

Webb EK, Pearman GI, Leuning R, 1980. Correction of flux measurements for density effects due to heat and water-vapor transfer. Quarterly Journal of the Royal Meteorological Society, 106: 85–100.

Wilczak JM, Oncley SP, Stage SA, 2001. Sonic anemometer tilt correction algorithms. Boundary-Layer Meteorology, 99: 127–150.

Wilson JD, Sawford BL, 1996. Review of Langrangian stochastic models for trajectories in the turbulent atmosphere. Boundary-Layer Meteorology, 78: 191–210.

Xu SY, Gao YX, 1962. Monsoon phenomena in Tibetan Plateau. Acta Geographica Sinica, 28(2): 111–123.

Xu XD, Chen LS, Zhou MY, 2002. The Second Tibetan Plateau Experiment of Atmospheric Sciences: TIPEX-GAME/TIBET. Beijing, China: Meteorological Press, pp. 236.

Yang K, Chen YY, Qin J, 2009. Some practical notes on the land surface modeling on the Tibetan Plateau. Hydrology and Earth System Sciences, 13: 687–701.

Yang K, Koike T, Ishikawa H, *et al.*, 2004. Analysis of the surface energy budget at a site of GAME/Tibet using a single-source model. Journal of the Meteorological Society of Japan, 82(1): 131–153. DOI: http://www.doi.org/10.2151/jmsj.82.131.

Yang K, Koike T, Ishikawa H, *et al.*, 2008. Turbulent flux transfer over bare-soil surfaces: Characteristics and parameterization. Journal of Applied Meteorology and Climatology, 47: 276–290.

Yang K, Koike T, Yang D, 2003. Surface flux parameterization in the Tibetan Plateau. Boundary-Layer Meteorology, 116: 245–262.

Yang K, Koike T, Ye B, *et al.*, 2005. Inverse analysis of the role of soil vertical heterogeneity in controlling surface soil state and energy partition. Journal of Geophysical Research, 110(D8): D08101. DOI: 10.1029/2004JD005500.

Yang K, Wang JM, 2008. A temperature prediction-correction method for estimating surface soil heat flux from soil temperature and moisture data. Science in China (Series D: Earth Sciences), 51(5): 721–729.

Yeh DZ, Gao YX, 1979. The Meteorology of the Qinghai–Xizang (Tibet) Plateau. Beijing: Science Press, pp. 278.

Yeh TC, Dao S, Li M, 1957. The abrupt change of circulation over the northern hemisphere during June and October. In: Rossy Memorial Volume. The Atmosphere and the Sea in Motion. The Rockefeller Institute Press, pp. 249–267.

Zhang JJ, Zhu BZ, Zhu FK, *et al.*, 1988. Advances in the Qinghai-Xizang Plateau Meteorology. Beijing: Science Press, pp. 268.